Available online at www.sciencedirect.com

ScienceDirect

Procedia Structural Integrity 80 (2026) 117–129

Structural Integrity Procedia

www.elsevier.com/locate/procedia

Fracture, Damage and Structural Health Monitoring

Yield Criterion for a Surface-Based Gyroid Structure: a Homogenization Approach

Mauro Giacalone[a*], Nicolò Lodini[a], Sara Mantovani[a], Angelo Caiani[b]

[a] *University of Modena and Reggio-Emilia, Department of Engineering "Enzo Ferrari", Via Vivarielli 10, 41124 Modena, Italy*
[b] *Ferrari SPA, Via Abetone Inferiore 4, 41053 Maranello, Italy*

Abstract

Cellular structures based on Triply-Periodic Minimal Surfaces are a popular option in the design of load bearing structures, because of their high, yet tunable, mechanical properties. Additive Manufacturing has made these structures feasible in a finished product, increasing their popularity even more.
The simulation of large components which include these structures usually require high computational costs if the effective geometry of the lattice is included in the model. This problem may be solved by adopting a homogeneous material equivalent to the effective lattice. Many techniques have been developed for the homogenization of the elastic properties of lattice structures, but much less is known about their resistance. A yielding criterion is required to determine the initial collapse of these structures with the limited set of information provided by the homogenized material.
This paper proposes a criterion to determine the yielding of periodic structures subject to multi-axial loading conditions. This criterion is applied to the surface based Gyroid at varying relative density. Finite Element methods will be performed in linear elastic conditions to link the macroscopic loads on an infinite lattice to the failure conditions of the material within the unit cell.

Keywords: Type your keywords here, separated by semicolons ;

* Corresponding author. Tel.: +39-059-205-6280.
E-mail address: mauro.giacalone@unimore.it

10.1016/j.prostr.2026.02.011

1. Introduction

Lattice structures are increasingly adopted in engineering applications, enabled by the widespread diffusion of additive manufacturing technologies, which allow the production of lightweight, high-performance components with unprecedented design freedom. In addition, Triply-Periodic Minimal Surfaces (TPMS) structures have gained attention in the scientific community for their potential use both in thermal and structural applications [1].
The accurate numerical modelling of such structures with a fine discretization may be computationally prohibitive due to their intricate geometries. To address these large-scale simulations, homogenization techniques have emerged as a practical solution, as these techniques approximate the effective behaviour of heterogeneous materials, providing engineering-relevant results at a manageable computational expense.
The homogenization of elastic properties in composite and cellular materials has been widely investigated with numerical techniques. For instance, Sun et al. [2] proposed a Representative Volume Element (RVE)-based approach employing periodic boundary conditions and energy equivalence principles to determine the elastic properties of polymer-matrix composites. Similarly, numerical homogenization has been used to predict the Young's modulus of periodic lattices [3], [4]. Bean et al. [5] applied this approach to derive a power-law relationship between the elastic modulus in the principal loading direction and the relative density. More recently, Defanti et al. [Defanti2024] exploited the full geometric and elastic symmetries of the gyroid structure to formulate an exponential law describing the dependence of the elastic modulus on the relative density [6].

The homogenization of the resistance of porous materials has first examples in foams. Gibson et al. [7] introduced a yield surface derived from an idealized foam cell. Deshpande and Fleck [8] subsequently proposed a phenomenological isotropic yield criterion, incorporating a quadratic dependence on both the effective von Mises stress and the mean stress, with a material parameter that recovers the classical von Mises yield criterion in the limiting case. Miller [9] extended the Drucker–Prager criterion to enable independent control over plastic compressibility, accounting for both linear and quadratic pressure sensitivities and allowing for asymmetric responses under tension and compression.
Additional studies further elucidated the complexities of yielding in cellular materials, with efforts that have primarily focused on beam-based lattices. Deshpande et al. [10] demonstrated, through FE analysis on the octet-truss lattice, that an extended version of Hill's anisotropic yield criterion, with a quadratic term in mean stress, effectively captures the pressure sensitivity of yielding. Experimental work by Doyoyo and Wierzbicki [11], using butterfly specimens of aluminum foams, led to the formulation of an isotropic yield surface capturing asymmetric uniaxial behavior.
Several studies have proposed numerical and analytical methods for predicting their effective yield behavior. For example, Park et al. [12] introduced a numerical homogenization framework specifically tailored to strut-based lattices, incorporating joint stiffening effects, while Arabnejad et al. [13] employed asymptotic homogenization to derive analytical yield criteria.
In the context of TPMS lattices, the characterization of yield behavior through homogenization has been addressed in a limited number of studies. Lee et al. [14] demonstrated that the multiaxial yield response of Schwarz Primitive TPMS foams is best described by an extended Hill anisotropic yield criterion, whereas classical isotropic models, such as the Deshpande–Fleck formulation, fail to accurately capture plastic behavior under combined loading conditions. Baghous et al. [15] proposed a yield criterion for Schoen's IWP-s TPMS structure, which accurately describes plastic behavior under multiaxial loading but is limited to IWP-s and was not calibrated for biaxial stress states. The model considers relative densities ($\boldsymbol{\rho/\rho_s}$) of 7%, 13%, 18% and 28%, but does not provide a universal scaling law. Later, Baghous et al. [16] generalized the approach to multiple sheet-based TPMS topologies, including Gyroid, with biaxial loading calibration, but the criterion is valid only for a single ρ/ρ_s. Recently, Nguyen-Van et al. [17]developed a surrogate model to predict the local stress field within Gyroid TPMS lattices. Their approach is based on a polynomial function that approximates the stress state of each element as a function of normalized wall thickness, Poisson's ratio, and the loads applied to the lattice structure. The yield behavior can be derived knowing the yield stress computed via the surrogate of each element. However, a homogenized yield criterion was not provided.
The present work focuses on the sheet based Gyroid and addresses these limitations by developing a yield criterion which is applicable across a ρ/ρ_srange between 0.097 to 0.916, considering multi-axial loading. The model was obtained from numerical simulations on the Gyroid unit cell with periodic boundary conditions. Given that yield surfaces exhibited an elliptical-like shape, this criterion was formulated using a super-elliptical equation, similarly to what was done in previous works to model the yield surface of two-dimensional metal sheets [18], [19], [20], [21],

[22]. The following lines will show the main steps for the numerical modelling of the Gyroid, as well as the steps that were taken to tailor the proposed yield criterion to the various ρ/ρ_s. Results will show a comparison between the numerically derived results, and the predictive model, showing errors below 33%. The proposed model may hopefully help the designers in reducing the computational cost of numerical validation tests of components including a graded gyroid structure.

2. Geometry Modeling and Finite Element Analysis

2.1. Geometry Creation

Gyroid is a Triply-Periodic Minimal Surface (TPMS) cell approximated with the implicit equation:

$$\left[cos\left(\frac{2\pi x}{l_x}\right)sin\left(\frac{2\pi y}{l_y}\right)+cos\left(\frac{2\pi y}{l_y}\right)sin\left(\frac{2\pi z}{l_z}\right)+cos\left(\frac{2\pi z}{l_z}\right)sin\left(\frac{2\pi x}{l_x}\right)\right]^2-a^2=0 \quad (1)$$

where $\boldsymbol{l_x}$, $\boldsymbol{l_y}$ and $\boldsymbol{l_z}$ are the cell sizes along the three coordinates. The level parameter $\boldsymbol{a}$ is directly connected to the relative density ($\boldsymbol{\rho/\rho_s}$) of the gyroid. This connection may be approximated as linear, and may be expressed as:

$$\frac{\rho}{\rho_s}=1.5a \quad (2)$$

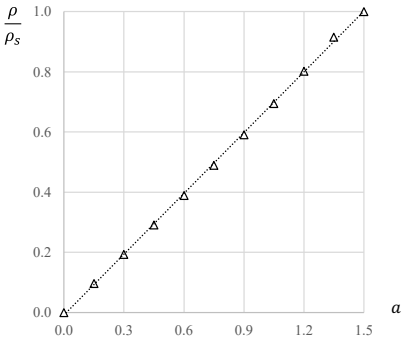

Figure 1 Influence of level parameter a on the relative density

The FE model of the gyroid was created by exploiting all the possible rotational symmetries within the unit cell. Once the relative density is chosen, the implicit equation was used to generate the fundamental patch of Figure 2a, corresponding to 1/48 of the entire unit cell. This patch was then discretized with first order, tetrahedral elements. A planar reflection and a rotation generate the part in Figure 2b. This part covers the whole stress state within the unit cell, as the stress state of the remaining of the unit will replicate the stress state within this part.

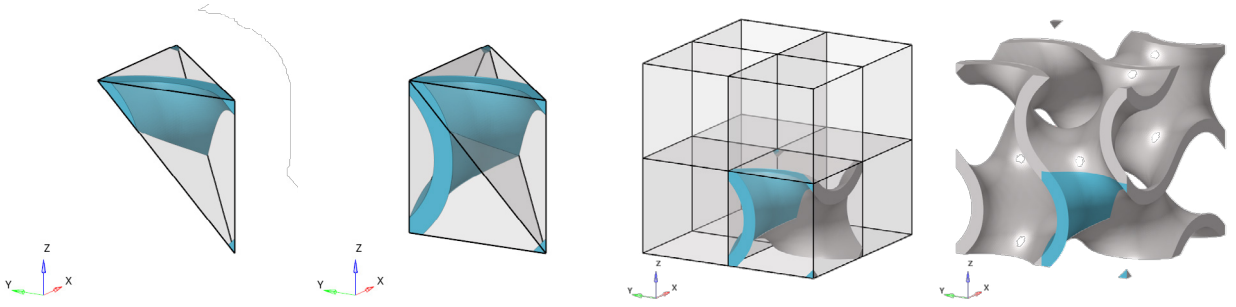

(a) (b) (c) (d)

Fig. 2 (a) Fundamental patch of the gyroid, (b) representative volume for stress evaluation, (c) 1/8 of the unit cell, (d) complete unit cell

Two more rotations lad to the 1/8 of the unit cell in Figure 2c, which finally was elaborated to obtain the complete unit cell (Figure 2d). This study considered cubic unit cells with a side of 1mm. Nine values of the level parameter a were chosen, equally spacing the [0-1.5] range. This led to the generation of nine unit cells with different relative densities. The fundamental patch for each density was created by using MathMod10, while all the meshing of the part, and the transformations to obtain the complete cell were done with Altair®HyperMesh.

3. FE Setup

To simulate a unit cell within an infinite lattice domain, nodal displacements on the external faces must mimic the surrounding periodic structure. This was achieved using Periodic Boundary Conditions (PBC). Following Mizzi et al. [23], constraint equations were applied between geometrically paired nodes on unit cell opposite faces, thanks to the periodic mesh. For clarity, consider the xy-plane (Figure 3a). The used constraint equations between paired nodes are:

$$\begin{aligned} u_B &= u_A + l\varepsilon_x \\ v_B &= v_A + l\gamma_{xy} \\ u_D &= u_C + l\gamma_{xy} \\ v_D &= v_C + l\varepsilon_y \end{aligned} \tag{3}$$

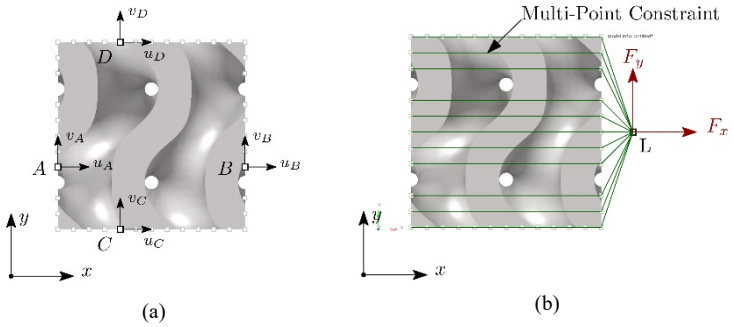

Figure 3 (a) Displacements of opposing boundary nodes, (b) Imposed Multi-Point Constraint along x-direction

Where, u and v are the nodal displacements along the x and y directions, respectively; l is the unit cell length, ε_x and ε_y are the normal strains, and γ_{xy} is the shear strain.

Satisfying Equation (3) ensures that the model captures the mechanical influence of the infinite lattice domain [6]. Equation (3) were extended to include displacements on all six faces of the unit cell. The extended equations were enforced on the unit cell by using Multi-Point Constraints (Figure 3b). The second term in the right members of Equation (3) were enforced by adding nine additional degrees of freedom, spread between three auxiliary nodes, one on each coordinate axis. One of the three auxiliary nodes is shown in Figure 3b.

The three auxiliary nodes are helpful to impose uniform stress on the unit cell. For example, to apply an axial stress along the x axis (σ_x) a force F_x mmust be applied to the auxiliary node on the x axis, so that:

$$\sigma_x = \frac{F_x}{A} \tag{4}$$

Where: A is the face area of the unit cell. Other uniform stresses may be applied in the same fashion.

The PBC scheme is efficient in eliminating the three rigid rotations of the unit cell, but doesn't restrain its three rigid translations. These residual rigid motions were impeded by fixing one node at the center of the unit cell.

The FE simulations adopted an isotropic material within the unit cell, with Young Modulus equal to 1, and Poisson's ratio equal to 0.3. Six simulations were conducted (Figure 4), each with a distinct stress configuration, to assess the mechanical response under simple loading scenarios. The applied stress states are summarized in Table 1. Under the assumption of linear elasticity, which typically occurs before the yielding of the material, the six uniform stresses was combined through superposition effect to obtain a generalized stress state on the lattice. The obtained results served as the basis for deriving the numerical yield surface.

The six simulations were applied to the FE models of the unit cell at nine densities. A total of 54 FE simulations were

performed in this study.

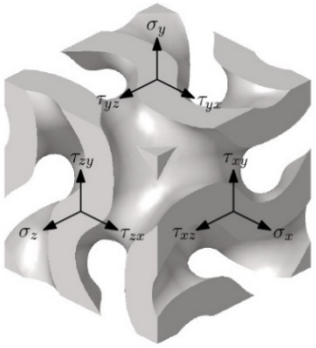

Figure 4 Representation of stress components applied to the periodic unit cell

Table 1 Fundamental loadcases

	Imposed Stress [MPa]					
Loadcase name	σ_x	σ_y	σ_z	τ_{xy}	τ_{yz}	τ_{xz}
Sx	1	0	0	0	0	0
Sy	0	1	0	0	0	0
Sz	0	0	1	0	0	0
Txy	0	0	0	1	0	0
Tyz	0	0	0	0	1	0
Txz	0	0	0	0	0	1

4. Mesh sensitivity analysis

The FE model of the Gyroid unit cells was obtained with first-order tetrahedral elements. To ensure numerical accuracy while maintaining computational efficiency, a mesh convergence study was conducted by evaluating the resulting von Mises stress. The reference unit cell for the study was chosen with a relative density of 0.49, which is halfway between the highest and lowest densities considered in this study.

Table 2 Results from mesh sensitivity analysis

Element size [mm]					Sxx loadcase		Tyz loadcase	
Min	Max	# Nodes	# Elements	CPU Time [s]	$\sigma_{vM,max}$ [MPa]	Δ [%]	$\sigma_{vM,max}$ [MPa]	Δ [%]
0.080	0.080	6106	3.07 E+04	27	4.39	-32.00	6.49	-23.52%
0.040	0.040	48798	2.70 E+05	192	5.66	-12.34	7.97	-6.04%
0.020	0.020	399722	2.34 E+06	1757	6.10	-5.55	8.32	-1.92%
0.010	0.020	582490	3.22 E+06	5561	6.38	-1.19	8.29	-2.29%
0.008	0.020	775694	4.23 E+06	8178	6.45	0.00	8.48	0.00%
0.004	0.020	6436766	3.90 E+07	66776	6.53	1.19	8.65	2.03%

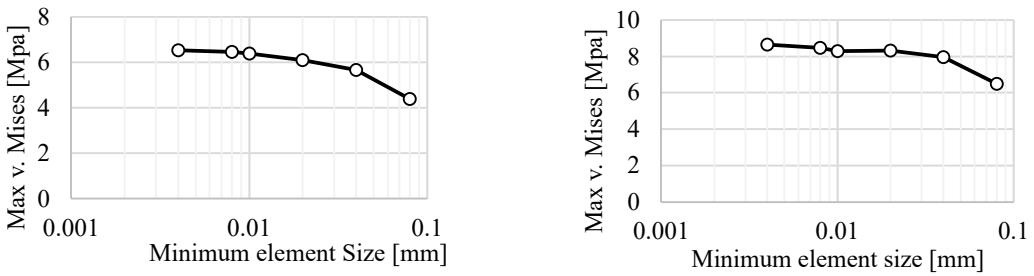

Fig. 5. Convergence of loadcases Sxx and Tyz

A uniform element size was selected for the whole unit cell when the element size was greater than 0.02. For smaller

sizes, a uniform mesh would have led to an excessive number of nodes. Therefore, a minimum element size was chosen for the faces of the gyroid, while the element size was increased inside the gyroid walls. This choice aims at capturing the stresses accurately where needed, while containing the number of nodes in the model. The minimum and a maximum element size are shown in Table 2, along with the details on the model size and computational time. The FE solver computed the von Mises stress $\sigma_{vM,max}$ for all fundamental loadcases. For brevity, only the loadcases Sxx and Tyz are presented. Convergence was considered achieved when successive mesh refinements produced a variation in $\sigma_{vM,max}$ stress lower than 2%. This threshold is considered as an optimal compromise between the accuracy of the results and the computational effort.
The results converged with a minimum mesh size of 0.008mm. This mesh size was adopted for all the FE simulations on the Gyroid unit cells, for all the relative densities in this study.

5. Yield Criterion Construction

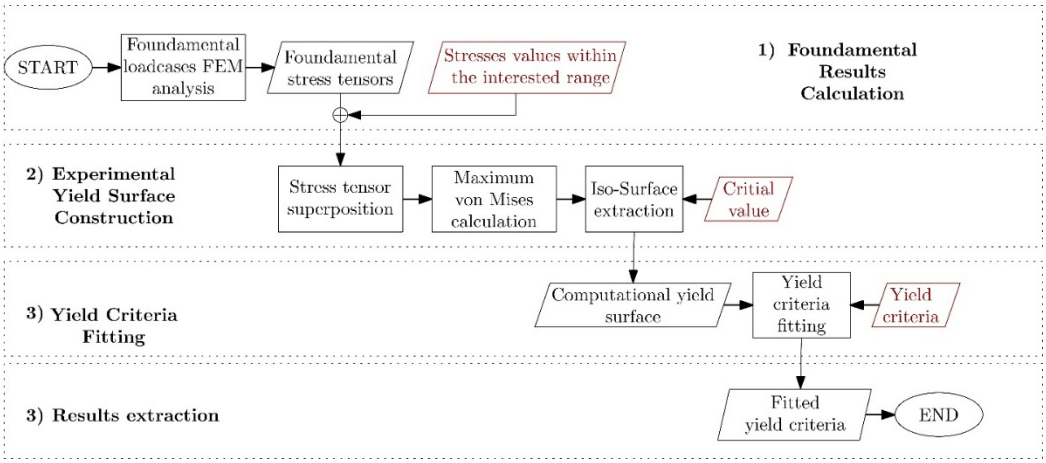

Figure 6 Workflow to determine the proposed yield criterion

Figure 6 shows the path towards the construction of the yield criterion in this study. It all started with the results of the FE simulations, which calculated the full stress tensors at each element in the fundamental patch in Figure 2b. These stresses will be representative of the stresses in the whole unit cell.

Table 3 Possible stress combinations for the three generalized stress conditions

Loading condition	Imposed Stress [MPa]					
	σ_x	σ_y	σ_z	τ_{xy}	τ_{yz}	τ_{zx}
Triaxial	[-5,5]	[-5,5]	[-5,5]	0	0	0
Pure shear	0	0	0	[-5,5]	[-5,5]	[-5,5]
Complete plane	[-5,5]	[-5,5]	0	[-5,5]	0	0

After the run of the six fundamental stress states on the unit cell, three generalized stress conditions were chosen for the Gyroid:

a) a Triaxial state, in which the unit cell is loaded with uniform axial stresses only.
b) a Pure shear state, where the gyroid undergoes a pure shear along the three planes.
c) a Complete plane stress state, with axial stresses and shear on the x-y plane.

In each of the three conditions, the axial or shear stresses were varied between -5MPa and 5MPa, with an increment of 0.1, reaching a total of more than 130 000 combinations per each condition. Table 4 summarises the average stress in the three conditions.

Each combination of stress in either of the three loading conditions represents a point in a three-dimensional space. At each of these points the average stress on the lattice was linked directly to the maximum equivalent von Mises stress within the material ($\sigma_{vM,max}$).
To do so, the stress within the elements of the unit cell were combined with linear superimposition. Then, the stress at each element was brought to the nodes with an arithmetic average:

$$\underline{\underline{\sigma_n}} = \frac{1}{N_e}\sum_{e=1}^{N_e}\underline{\underline{\sigma_e}} \tag{5}$$

where N_e is the total number of elements concurring to node n.
After averaging all the single stress components, the equivalent von Mises stress was calculated at each node. $\sigma_{vM,max}$ is the maximum von Mises stress among all the nodes.
The yielding of the lattice occurs when $\sigma_{vM,max}$ reaches the yield stress σ_y of the material of the lattice

$$\frac{\sigma_{vM,max}}{\sigma_y} = 1 \tag{6}$$

With the resulting data, a yield surface may be built, as the geometrical locus of all the points where condition (6) was met. An example of yield surface is shown in Figure 7. As was predictable, the yield surface for the Triaxial state in Figure 7a is limited even when the stress state becomes hydrostatic, unlike what happens for homogeneous materials.

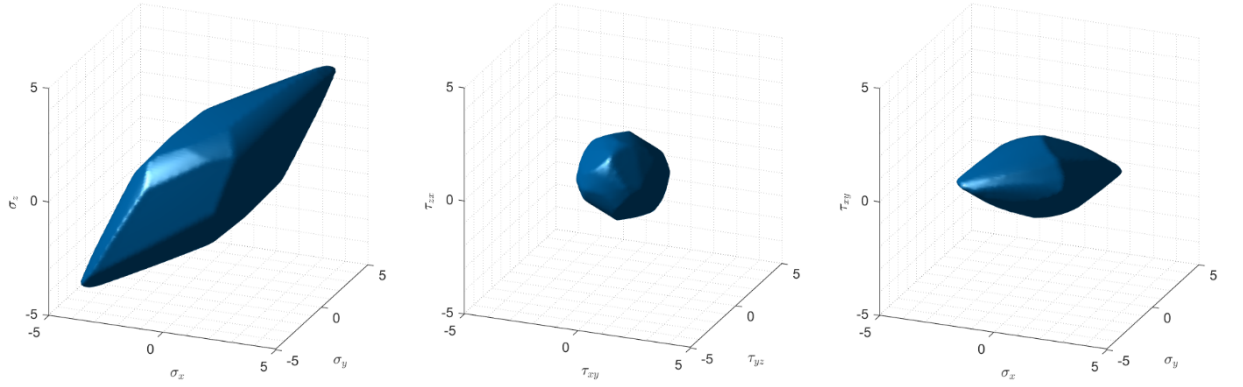

(a) (b) (c)

Figure 7 Yield surfaces ($\sigma_{vM,max}$ = 15 MPa) for the Triaxial (a), Triple Shear (b) and Complete Plane (c) conditions. $\rho/\rho_s = 0.489$.

Triple Shear seems to be the most critical stress condition, its ball-shaped yield surface (Figure 7b) contains the smallest volume of all the three conditions. The yield surface of the complete plane in Figure 7c is somehow between the two previous conditions. It remains quite small along the τ_{zx} axis, and is slightly elongated in the $\sigma_x - \sigma_y$ plane, along the direction of a plane hydrostatic state, much like what happens in the Triaxial condition. In all the stress conditions, the surfaces do not appear to be completely smooth, mostly because of the maximum operator, used to select $\sigma_{vM,max}$.
The study went on with the search for a model that could find the best fit with the data that were elaborated from the FE results. For the sake of simplicity, the model was chosen to be a function of the principal stresses on the lattice (σ_1, σ_2 and σ_3). The model is based on a super-ellipse equation:

$$\sigma_{eq} = \left(\left|\frac{\sigma_1 + \sigma_2 - a\sigma_3}{b}\right|^n + \left|\frac{\sigma_1 - a\sigma_2 + \sigma_3}{b}\right|^n + \left|\frac{-a\sigma_1 + \sigma_2 + \sigma_3}{b}\right|^n + \left|\frac{\sigma_1 - \sigma_2}{c}\right|^n + \left|\frac{\sigma_2 - \sigma_3}{c}\right|^n + \left|\frac{\sigma_3 - \sigma_1}{c}\right|^n\right)^{\frac{1}{n}} \tag{7}$$

The model is made up of six terms, each describing a couple of parallel planes in the σ_1–σ_2–σ_3 space. The numerator of each term defines the orientation of the couple of planes, while the denominator determines the distance between the two planes. The model is made of two triplets to account for the three-fold rotational symmetry of the Gyroid with respect to the first diagonal of the cube.

The first three terms regulate the effect of hydrostatic stress, the inclination of the planes is mostly determined by the coefficient a, while b is linked to the overall resistance of the lattice to a hydrostatic load.
The remaining three terms are linked to the contribution of deviatoric stress, this time, the inclination of the three planes is much simpler, and a third coefficient c, is added to account the resistance, independently from the hydrostatic stress.
Finally, an exponent n is applied to the six terms of the equation, as well as to σ_{eq}, much like what happens for the equivalent von Mises stress. This coefficient regulates the sharpness of the features of the yield surface resulting from the model. In this study, n is always greater than 2, meaning that the resulting yield surface is always sharper than a 2nd order ellipsoid.
By considering the coefficients a, b, c and n as functions of the relative density ρ/ρ_s, the model becomes able to predict the equivalent stress for any sheet-based Gyroid. Or at least, it is intended to become so.
The exponent n was chosen to be linearly decreasing with the relative density:

$$n\left(\frac{\rho}{\rho_s}\right) = 12 - 6\left(\frac{\rho}{\rho_s}\right) \tag{8}$$

The remaining three coefficients were calculated with an optimization. For each of the three stress conditions, a coefficient of determination (R^2) was determined between the maximum von Mises from the FE simulations ($\sigma_{vM,max}$) and the equivalent of stress in the presented model (σ_{eq})

$$R^2 = 1 - \frac{\sum_i \left(\sigma_{eq,i} - \sigma_{vM,max,i}\right)^2}{\sum_i \left(\sigma_{vM,max,i} - \overline{\sigma_{vM,max}}\right)^2} \tag{9}$$

Where i represents the i-th combination in the given generalized stress condition, and $\overline{\sigma_{vM,max}}$ is the mean value of the FE calculated $\sigma_{vM,max}$ at all combinations. The objective of the optimization was to maximize R^2, while the coefficients a, b and c were the variables of the optimization.
The optimization was carried out with a MATLAB routine, which explored all the three stress conditions, and all the nine relative densities in this study. The optimization returned three coefficients a, b and c, one for each stress condition. c was chosen from the Triple shear condition, while a and b were chosen from the Triaxial condition. Finally, the values of the coefficients were approximated with functions of ρ/ρ_s to obtain a unified model for the equivalent stress within the lattice.

6. Results

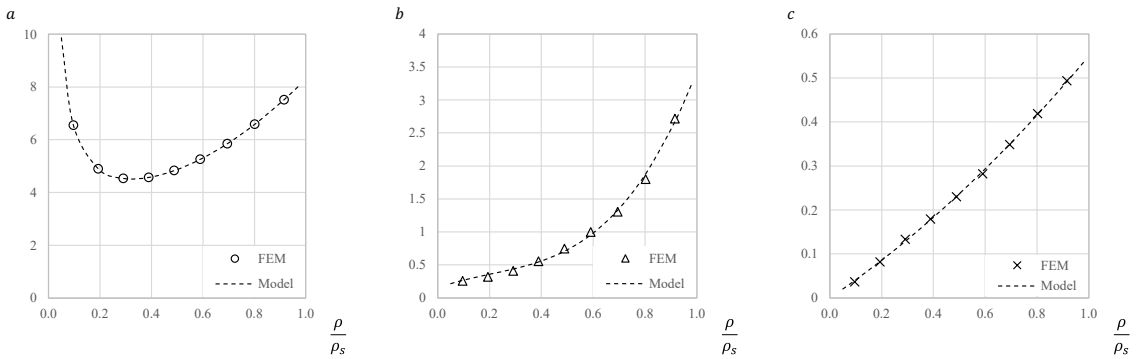

Figure 8 Coefficients of the super-elliptical model over the relative density

Figure 8 shows the main coefficients of the presented model, as resulted from the optimizations. These coefficients are best approximated with the functions:

$$a\left(\frac{\rho}{\rho_s}\right) = 0.347\left(\frac{\rho}{\rho_s}\right)^{-1} + 5.03\left(\frac{\rho}{\rho_s}\right)^{2} + 2.91$$
$$b\left(\frac{\rho}{\rho_s}\right) = 4.83\left(\frac{\rho}{\rho_s}\right)^{3} - 3\left(\frac{\rho}{\rho_s}\right)^{2} + 1.45\left(\frac{\rho}{\rho_s}\right) + 0.15 \quad (10)$$
$$c\left(\frac{\rho}{\rho_s}\right) = 0.152\left(\frac{\rho}{\rho_s}\right)^{2} + 0.408\left(\frac{\rho}{\rho_s}\right)$$

These results, united to condition (9), complete the model for the equivalent stress within the Gyroid.
It is worth noting that the coefficients b and c are monotonically increasing with ρ/ρ_s, therefore –as one could expect– lattices with lower density are less resistant to external loads. In addition, c tends to zero as ρ/ρ_s tends to zero, meaning that a lattice with extremely low relative density would collapse even with the slightest deviatoric stress.
On the other hand, b does not tend to zero as ρ/ρ_s tends to zero, meaning that a slight hydrostatic load may not lead to the collapse of a Gyroid with extremely low ρ/ρ_s. These results need a further and deeper study, focused mainly on ρ/ρ_s below 10%, in order for it to be confirmed.
Figure 9 compares the results of the proposed model and the FE results in Triaxial condition. From the top left, to the bottom right, the figure shows a focus on three planes with $\sigma_y = 0$, $\sigma_x = 0$ and $\sigma_z = 0$, respectively, as well as an isometric view of a yield surface at $\sigma_{vM,max}$ = 40MPa. The plane views suggest a slight underestimation of $\sigma_{vM,max}$ under deviatoric stresses, while on the other hand, the iso-surface shows a slight overestimation of $\sigma_{vM,max}$ under pure hydrostatic stresses.

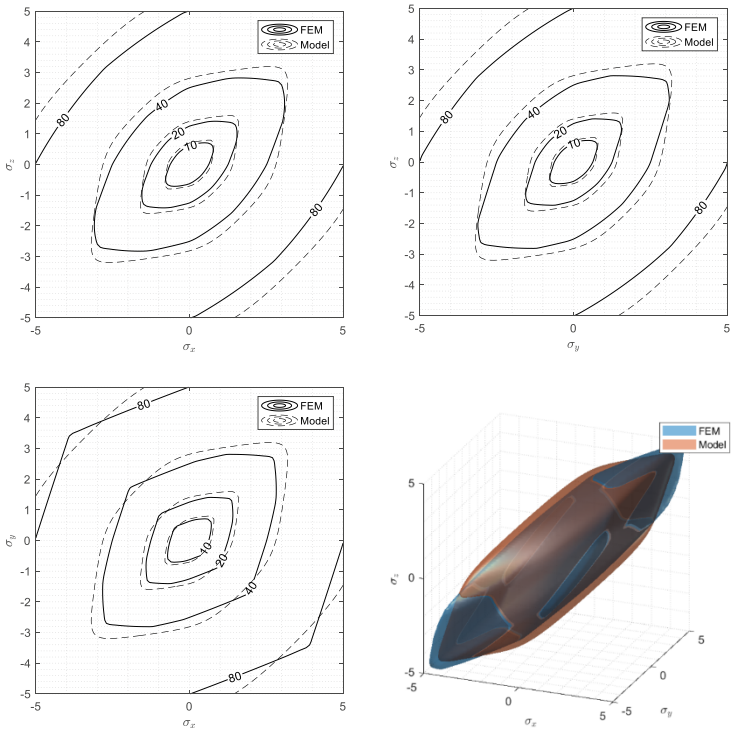

Figure 9 Comparison between FE results and proposed model for the triaxial case ($\rho/\rho_s = 0.194$). Iso-surfaces at $\sigma_{vM,max}$=40MPa.

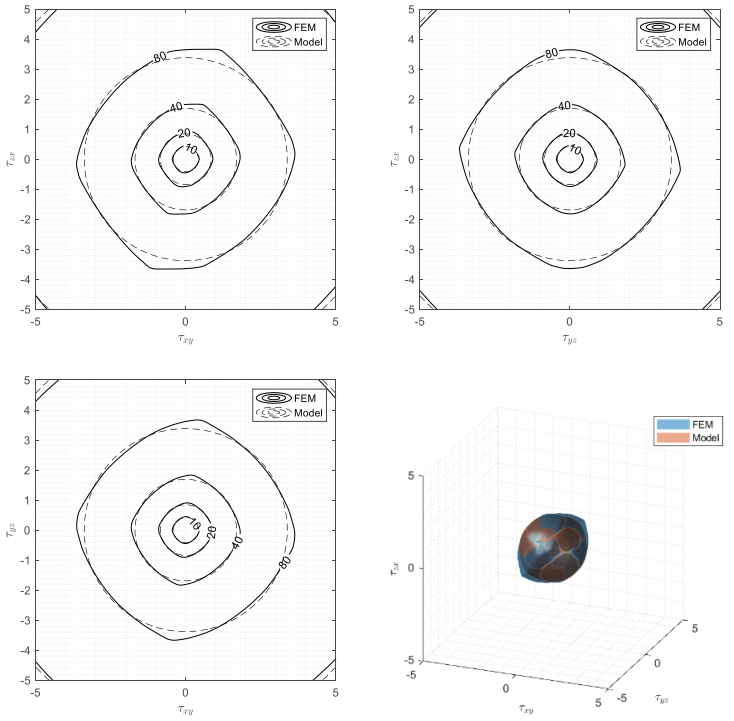

Figure 10 Comparison between FE results and proposed model for the triple shear case ($\rho/\rho_s = 0.194$). Iso-surfaces at $\sigma_{vM,max}$=40MPa.

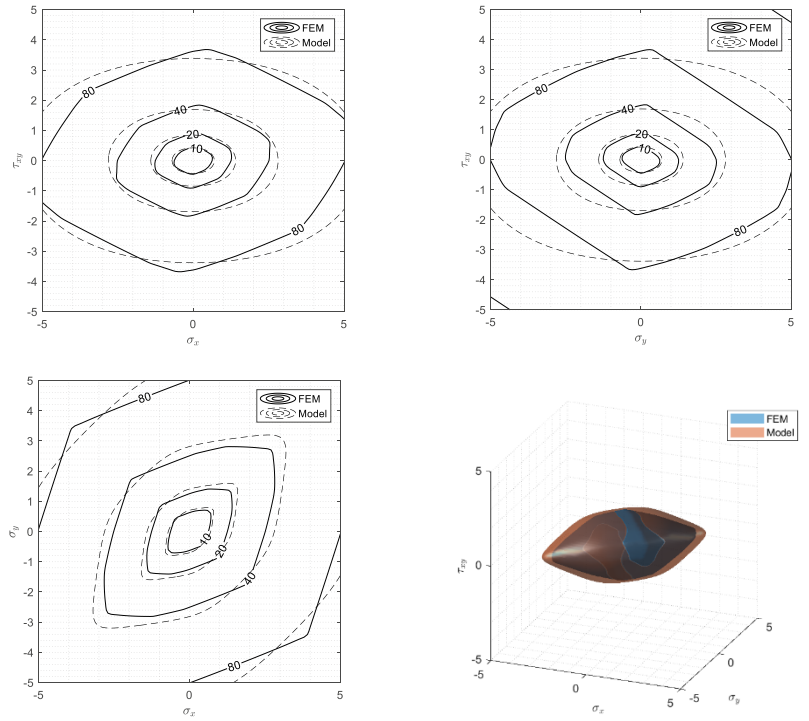

Figure 11 Comparison between FE results and proposed model for the complete plane case ($\rho/\rho_s = 0.194$). Iso-surfaces at $\sigma_{vM,max}$=40MPa.

Figure 10 shows a breakdown of the same lattice under the triple shear condition. At a ρ/ρ_s of 0.194, the iso-lines show that the proposed model follows the FE results, with some slight over-estimations and under-estimations. On accounting the Complete Plane condition shown in Figure 11, the model seems to generally under-estimate the FE results. This is mostly due to the fact that the coefficients of the proposed model were tailored mostly on the first two condition.

The proposed model was then tested for its accuracy, confronting once again the resulting σ_{id} with the $\sigma_{vM,max}$. The maximum overestimation (Δ_{max}) and the maximum underestimation (Δ_{min}) of $\sigma_{vM,max}$ were calculated and summarized in Table 4. The best performance is given in the triaxial condition, where the worst Δ_{max} reaches 21,6% and the worst Δ_{min} remains below 20%.

Table 4 Test results for the proposed equivalent of stress

Level parameter	ρ/ρ_s	Condition 1: Triaxial		Condition 2: Triple Shear		Condition 3: Complete plane	
		Δ_{max}	Δ_{min}	Δ_{max}	Δ_{min}	Δ_{max}	Δ_{min}
0.15	0.097	11.5%	-15.9%	9.2%	-21.6%	33.4%	-27.4%
0.30	0.194	12.3%	-16.2%	18.6%	-13.4%	20.0%	-23.2%
0.45	0.291	14.5%	-15.0%	35.7%	-1.5%	14.0%	-21.0%
0.60	0.389	19.1%	-12.8%	33.1%	-2.0%	14.9%	-18.9%
0.75	0.489	21.6%	-10.7%	23.5%	7.5%	18.5%	-16.8%
0.90	0.591	20.2%	-13.2%	27.6%	1.5%	15.1%	-16.6%
1.05	0.695	11.3%	-18.0%	21.8%	1.0%	12.8%	-19.7%
1.20	0.802	7.3%	-18.6%	25.0%	-1.0%	15.6%	-21.9%
1.35	0.916	7.8%	-14.8%	30.6%	-1.4%	20.8%	-20.1%

In the Triple shear condition, the model appears to be overconservative at densities between 30% and 70%, while at very low ρ/ρ_s may underestimate the FE result by as much as 21,6%. The Complete plane condition has its poorest performance at the lowest ρ/ρ_s, at which it yields a Δ_{max} of about 33%, and a Δ_{min} of about 27%. At all the remaining relative densities, the error between the super-elliptical model and the FE results lies below 24%.

Overall, the proposed model presents fair results at ρ/ρ_s between 0.2 and 0.7, although with some slight exceptions. Some further studies may further improve the super-elliptical model of equation (7), exploring in higher detail the densities above 0.7 and below 0.2. Some further studies may be also done to explore more intense loading conditions, as well as different stress combinations that may typically occur in practice.

7. Conclusions

The present work proposed a yield criterion for sheet-based Gyroid lattice structures under multiaxial loads. This yield criterion is meant to be applied to additively manufactured metal structures.

Supposing that the initial yielding of the lattice structure occurs when the maximum equivalent von Mises stress within the lattice ($\sigma_{vM,max}$) reaches the yield strength of the material, predictive model was adopted to link the external stresses to $\sigma_{vM,max}$. This model is based on a super-ellipse like equation.

Using Finite Element (FE) simulations under the hypothesis of linear elasticity, superposition principle was applied to cover multiple stress combinations on the unit cell, starting from six fundamental loading conditions. The super-elliptical model was tailored to match the results of FE simulations with an optimization. Then, the experiment was repeated covering various relative densities (ρ/ρ_s) of the Gyroid, aiming to obtain a unified, predictive model for the Gyroid structure.

Results show a fair accordance between the proposed model and FE results, specially at ρ/ρ_s between 0.2 and 0.7. The presented model exhibited in the proposed test cases, a maximum overestimation of 35.7% and a maximum underestimation of 27.4% of the FE results.

The proposed model may hopefully help the designer in simplifying the design and virtual validation of structures

which adopt a uniform or a graded Gyroid structure, although some more studies may be required to further refine the predictive model, and an experimental validation could be required to better tailor the model to as-manufactured structures.

Acknowledgements

This work has been supported by the project "GOALS, Green Optimizations by Additive-manufactured Lightweight Structures", Project 20228PFA89, CUP J53D23001980006, Progetti di Ricerca di Rilevante Interesse Nazionale PRIN 2022, funded under the National Recovery and Resilience Plan (NRRP), Mission 4 Component C2 Investment 1.1 by the European Union – NextGenerationEU.

This work was also supported by the University of Modena and Reggio Emilia with "Fondo di Ateneo per la Ricerca 2022 per il finanziamento di piani di sviluppo dipartimentale nell'ambito della ricerca" (FARD 2024).

8. References

[1] F. Torri *et al.*, "Evaluation of TPMS Structures for the Design of High Performance Heat Exchangers," in *SAE Technical Papers*, SAE International, 2023. doi: 10.4271/2023-24-0125.

[2] C. T. Sun and R. S. Vaidya, "PREDICTION OF COMPOSITE PROPERTIES FROM A REPRESENTATIVE VOLUME ELEMENT."

[3] E. Andreassen and C. S. Andreasen, "How to determine composite material properties using numerical homogenization," *Comput Mater Sci*, vol. 83, pp. 488–495, Feb. 2014, doi: 10.1016/j.commatsci.2013.09.006.

[4] D. Li, N. Dai, Y. Tang, G. Dong, and Y. F. Zhao, "Design and Optimization of Graded Cellular Structures with Triply Periodic Level Surface-Based Topological Shapes," *Journal of Mechanical Design*, vol. 141, no. 7, Jul. 2019, doi: 10.1115/1.4042617.

[5] P. Bean, R. A. Lopez-Anido, and S. Vel, "Numerical Modeling and Experimental Investigation of Effective Elastic Properties of the 3D Printed Gyroid Infill," *Applied Sciences (Switzerland)*, vol. 12, no. 4, Feb. 2022, doi: 10.3390/app12042180.

[6] S. Defanti, M. Giacalone, S. Mantovani, and E. Tognoli, "Dimensional and mechanical assessment of gyroid lattices produced in aluminum by laser powder bed fusion," *Meccanica*, Mar. 2024, doi: 10.1007/s11012-024-01854-7.

[7] L. J. Gibson, M. F. Ashby, J. Zhang, and T. C. Triantafillou, "FAILURE SURFACES FOR CELLULAR MATERIALS UNDER MULTIAXIAL LOADS-I. MODELLING," 1989. doi: https://doi.org/10.1016/S0020-7403(89)80001-3.

[8] V. S. Deshpande and N. A. Fleck, "Isotropic constitutive models for metallic foams." [Online]. Available: www.elsevier.com/locate/jmps

[9] R. E. Miller, "A continuum plasticity model for the constitutive and indentation behaviour of foamed metals," 2000.

[10] V. S. Deshpande, N. A. Fleck, and M. F. Ashby, "EEective properties of the octet-truss lattice material," 2001. [Online]. Available: www.elsevier.com/locate/jmps

[11] M. Doyoyo and T. Wierzbicki, "Experimental studies on the yield behavior of ductile and brittle aluminum foams." [Online]. Available: www.elsevier.com/locate/ijplas

[12] S. I. Park and D. W. Rosen, "Homogenization of mechanical properties for material extrusion periodic lattice structures considering joint stiffening effects," *Journal of Mechanical Design*, vol. 140, no. 11, Nov. 2018, doi: 10.1115/1.4040704.

[13] S. Arabnejad and D. Pasini, "Mechanical properties of lattice materials via asymptotic homogenization and comparison with alternative homogenization methods," *Int J Mech Sci*, vol. 77, pp. 249–262, 2013, doi: 10.1016/j.ijmecsci.2013.10.003.

[14] D. W. Lee, K. A. Khan, and R. K. Abu Al-Rub, "Stiffness and yield strength of architectured foams based on the Schwarz Primitive triply periodic minimal surface," *Int J Plast*, vol. 95, pp. 1–20, Aug. 2017, doi: 10.1016/j.ijplas.2017.03.005.

[15] N. Baghous, I. Barsoum, and R. K. Abu Al-Rub, "The effect of Lode parameter on the yield surface of

Schoen's IWP triply periodic minimal surface lattice," *Mechanics of Materials*, vol. 175, Dec. 2022, doi: 10.1016/j.mechmat.2022.104473.

[16] N. Baghous, I. Barsoum, and R. K. Abu Al-Rub, "Generalized yield surface for sheet-based triply periodic minimal surface lattices," *Int J Mech Sci*, vol. 252, Aug. 2023, doi: 10.1016/j.ijmecsci.2023.108370.

[17] S. Nguyen-Van, G. Manogharan, L. H. Huang, and J. A. Norato, "Surrogate models of stress for triply periodic minimal surface lattices," *Comput Methods Appl Mech Eng*, vol. 444, Sep. 2025, doi: 10.1016/j.cma.2025.118119.

[18] A. V. H. I. Dahlgren, "The Plasticity of an Isotropic Aggregate of Anisotropic Face-Centered Cubic Crystals," 1954. [Online]. Available: http://asmedigitalcollection.asme.org/appliedmechanics/article-pdf/21/3/241/6748715/241_1.pdf

[19] W. F. Hosford, "A Generalized Isotropic Yield Criterion," *J Appl Mech*, vol. 39, no. 2, pp. 607–609, Jun. 1972, doi: 10.1115/1.3422732.

[20] "Barlat1987_Crystallographic Texture, Anisotropic Yield Surfaces and Forming Limits of Sheet Metals", doi: https://doi.org/10.1016/0025-5416(87)90283-7.

[21] F. Barlat and J. Lian, "PLASTIC BEHAVIOR AND STRETCHABILITY OF SHEET METALS. PART h A YIELD FUNCTION FOR ORTHOTROPIC SHEETS UNDER PLANE STRESS CONDITIONS," 1989.

[22] M. Dutko, D. Perić, and D. R. J. Owen, "Universal anisotropic yield criterion based on superquadric functional representation: Part 1. Algorithmic issues and accuracy analysis," 1993.

[23] L. Mizzi, D. Attard, R. Gatt, K. K. Dudek, B. Ellul, and J. N. Grima, "Implementation of periodic boundary conditions for loading of mechanical metamaterials and other complex geometric microstructures using finite element analysis," *Eng Comput*, vol. 37, no. 3, pp. 1765–1779, Jul. 2021, doi: 10.1007/s00366-019-00910-1.